Design of a Lithium-ion Battery Pack for PHEV Using a Hybrid Optimization Method

Nansi Xue[1,*], Wenbo Du[1], Thomas A. Greszler[3], Wei Shyy[2], Joaquim R. R. A. Martins[1]

Ann Arbor, Michigan, USA

Abstract

This paper outlines a method for optimizing the design of a lithium-ion battery pack for hybrid vehicle applications using a hybrid numerical optimization method that combines multiple individual optimizers. A gradient-free optimizer (ALPSO) is coupled with a gradient-based optimizer (SNOPT) to solve a mixed-integer nonlinear battery pack design problem. This method enables maximizing the properties of a battery pack subjected to multiple safety and performance constraints. The optimization framework is applied to minimize the mass, volume and material costs. The optimized pack design satisfies the energy and power constraints exactly and shows 13.9 – 18% improvement in battery pack properties over initial designs. The optimal pack designs also performed better in driving cycle tests, resulting in 23.1 – 32.8% increase in distance covered per unit of battery performance metric, where the metric is either mass, volume or material cost.

Keywords: Lithium-ion, Optimization, Hybrid vehicle, Battery pack design

Contents

*Corresponding author: courtrun@umich.edu
[1]Department of Aerospace Engineering, University of Michigan
[2]Department of Mechanical Engineering, Hong Kong University of Science and Technology
[3]Saft America Inc., Cockeysville, MD

1. Introduction

Hybrid vehicles are becoming increasingly common as automakers make use of alternative energy storage systems to improve vehicle performance and efficiency [1, 2], and to reduce their environmental impact [3]. Among the alternative energy storage systems, lithium-ion batteries are a popular choice due to their high energy densities and cycling durability [4]. Plug-in hybrid electric vehicles (PHEV) incorporate these batteries to provide all-electric driving range for daily commuting. The main problem with lithium-ion batteries is that their energy density is orders of magnitude lower than that of gasoline. As such, the lithium-ion battery packs on PHEVs tend to be heavy, bulky and expensive. This limits the all-electric driving range the PHEV can sustain, and hence reduces the advantages of the hybrid drivetrain. Therefore, an optimally designed battery system is essential to maximize the potential benefits of PHEV.

Lithium-ion electrochemical modeling has been well studied in the past 20 years, with models of varying degrees of fidelity being introduced. Doyle and Newman [5] introduced a continuum formulation to model the ion transport and kinetics within an electrochemical cell. Equivalent circuit models simplify cell mechanisms and reduce a battery to a few parameters identified by simplified circuits [6, 7]. These models have been subsequently applied to analyze battery performance in electric vehicle operations [8, 9]. Ramadesigan et al. [10] provided a comprehensive overview of various model and simulation techniques of lithium-ion batteries from a system engineering perspective. A number of authors have examined the development and modeling of electrochemical energy storage systems for vehicle applications as well. Cooper [11] has examined the use of lead-acid battery for hybrid electric vehicles. Liaw and Dubarry [12] proposed a methodology to understand battery performance and life cycle through driving cycle and duty cycle analyses. This enables transfer between the laboratory and real-life battery testing by providing a realistic model to simulate battery performance using real-life test data [13].

While numerical models provide an understanding of the physics of battery operation, optimization algorithms provide the means to maximize the battery properties and performance in hybrid vehicle operations. Shahi et al. [14] applied a multi-objective optimization approach for the hybridization of a PHEV subject to Urban Dynamometer Driving Schedule (UDDS) and Winnipeg Weekday Duty Cycle (WWDC) drive cycle requirements. Wu et al. [15] described a methodology to minimize the drivetrain cost of a parallel PHEV by optimizing its component sizes. Hung and Wu [16] developed an integrated optimization strategy in which both the component sizing and control strategies are taken into consideration to maximize the energy capacity stored while minimizing the energy consumed for a given driving cycle. Optimization of combined component sizing and control strategies have been explored by Zou et al. [17] to study the hybridization of a tracked vehicle, and by Kim and Peng [18] for the design of fuel cell/battery hybrid vehicles. Darcovich et al. [19] extended lithium ion battery use to improve residential energy storage with micro-cogeneration by examining high-capacity cathode materials.

While power management, control strategies and component sizing all play key roles in achieving greater overall vehicle efficiency, a detailed optimization of PHEV battery packs has not been considered. Most of the earlier battery optimization works have focused on single-cell optimization, where the battery is optimized for maximum energy density [20, 21, 22, 23, 24]. More recent efforts have optimized the energy capacity of battery cells with respect to different power capacities by varying the applied current [25, 26]. Most optimization studies, however, have ignored the multitude of requirements due to hybrid vehicle operations. Specifically, the

battery pack has to satisfy: 1) voltage and current constraints for both safety reasons and to minimize power electronic cost, and 2) energy and power requirements for performance. To address these issues, we present a numerical framework to optimize the mass, volume and material costs of the battery pack, while satisfying all relevant requirements. By combining efficient numerical methods with existing battery models, waste attributed to sub-optimal pack design can be reduced. This type of analysis is especially important as electric vehicles become more mainstream and higher volume where small variation from the optimal solution, which may only result in slight overdesign (in terms of cost or volume), results in large penalties when compounded over a large quantity of vehicles. This type of analysis also provides a quick, cost effective design tool in the early phases of vehicle development - giving realistic guidelines on what is possible in terms of cost, size, and weight for a given battery chemistry.

In the following sections we explain the details of the numerical framework followed by the optimization results for a representative PHEV battery pack design. Using the optimization results we aim to demonstrate that the resulting battery pack is able to fulfill the various PHEV operation requirements most efficiently, hence maximizing the potential gains of PHEV operation. Finally, three federal test drive cycles are used to evaluate the performance of the battery designs by comparing the all-electric driving ranges.

2. Methodology

This section presents an overview of the optimization framework and the details of the individual components. An optimization problem has the general form:

$$\begin{aligned} &\text{minimize} \quad f(\boldsymbol{x}), \qquad\qquad f : \mathbb{R}^n \rightarrow \mathbb{R} \\ &\text{subject to} \quad \begin{cases} \boldsymbol{x}_{min} \leq \boldsymbol{x} \leq \boldsymbol{x}_{max} \\ c_j(\boldsymbol{x}) \leq 0 \quad j = 1, ..., m \\ \hat{c}_k(\boldsymbol{x}) = 0, \quad k = 1, ..., \hat{m} \end{cases} \end{aligned} \tag{1}$$

where $f(\boldsymbol{x})$ is the objective function to be optimized with respect to the bounded variables $\boldsymbol{x}$, and subject to inequality constraints $c(\boldsymbol{x})$ and equality constraints $\hat{c}(\boldsymbol{x})$.

The optimization process is an iterative one that repeatedly samples the design space to locate the optimal design point, as shown in Figure 1. Both gradient-free and gradient-based optimizers can be employed to solve the battery pack optimization problem. There are two main components to this numerical framework: 1) the numerical optimizers that determine the search direction and convergence criteria of the numerical processes, and 2) the objective function or battery model. The battery model can be further divided into cell model and pack model. The following subsections will explain each of these components in detail.

2.1. Optimization technique

The performance and properties of a single electrochemical cell is determined by morphological parameters such as the electrode porosity and thickness. Physically, the output of the cell should vary smoothly with these continuous variables, though the effects can be nonlinear. Gradient-based optimization methods are most apt at handling problems that have smooth design space and are convex near the optima. While the design at the cell level involves continuous variables, the battery layout (number of cells in series and parallel) at the pack level requires integer values, thus making the battery pack design a mixed-integer optimization problem. Gradient-free optimization methods do not require design space to be continuous or smooth, thus enabling

easier coupling with mixed-integer problems. However, the lack of gradient information tends to make gradient-free method less efficient than gradient-based method, and there is less confidence in the obtained results due to lack of mathematical optimality conditions. For the battery design problem specified here, we propose a hybrid optimization scheme that takes advantage of the the independence between the cell design and the pack design. The top half of Figure 1 shows the initial design phase during which a rudimentary optimization using a gradient-free optimizer is carried out to determine the optimal integer variables. Results from the gradient-free optimization are used as the starting point of the gradient-based optimization to obtain a refined cell design with respect to the continuous variables, as shown in the bottom half of Figure 1. The gradient-free optimizer minimizes the chance of finding a local minimum in the nonlinear design space and the gradient-based optimizer pinpoints the exactly location of the optimum. The hybrid optimization process takes advantage of the different niches of the two classes of optimizers to facilitate an efficient optimization process. The current optimization approach takes about a week of computational time to reach convergence, with the bulk of time spent in the gradient-free optimization. However, it should be noted that the gradient-free optimization can be parallelized and thus significantly shorten the computational time.

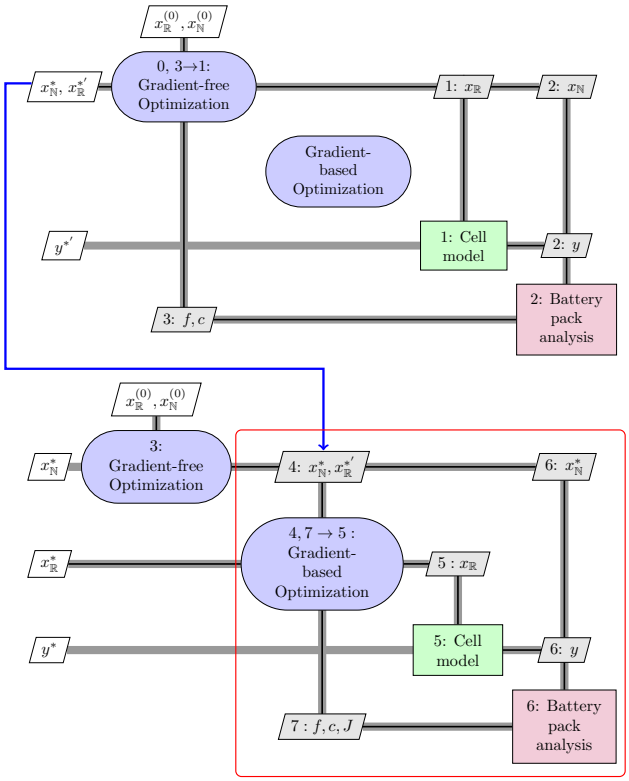

Figure 1: Extended design structure matrix for the optimization process [27]. Top: gradient-free optimization is used to determine value of integer variables and provide starting points for the gradient-based optimizations. Bottom: gradient-based optimization (shown in the red box) is used to fine-tune the continuous variables at the optimum

The overall battery pack problem is a nonlinear mixed-integer problem with constraints. The optimizer has to traverse a discontinuous constrained design space and handle nonlinear problems efficiently. For this reason we choose the augmented Lagrangian particle swarm optimization (ALPSO) method implemented within the pyOpt framework [28, 29]. The ALPSO algorithm is a stochastic, population-based method that employs a group of candidate solutions–known as particles–to identify the optimum [28]. These particles move about in the design space by updating their positions and velocities according to the following equations:

$$\begin{aligned} \boldsymbol{x}_{k+1}^{i} &= \boldsymbol{x}_{k}^{i} + \boldsymbol{V}_{k+1}^{i}\Delta t \\ \boldsymbol{V}_{k+1}^{i} &= w_0 \boldsymbol{V}_{k}^{i} + w_1 r_1 \left(\boldsymbol{p}_{k}^{i} - \boldsymbol{x}_{k}^{i}\right) + w_2 r_2 \left(\boldsymbol{p}_{k}^{g} - \boldsymbol{x}_{k}^{i}\right) \end{aligned} \tag{2}$$

where $\boldsymbol{x}_k^i$ is the position of the ith particle at iteration k, $\boldsymbol{V}_k^i$ is its velocity vector, Δt is the time step size, $\boldsymbol{p}_k^i$ is the position with the best objective function for particle i (particle best), and $\boldsymbol{p}_k^g$ is the global position with the best objective function for all the particles up to the kth iteration (global best). The movements of the particles are hence governed by their own movement history as well as the collective influence of the entire swarm. The weights, w_0, w_1 and w_2 are assigned to each component of the velocity update. They are bound by the following relations to ensure stability and to guarantee convergence [28]:

$$\begin{aligned} &0 < w_1 + w_2 < 4 \\ &\tfrac{w_1+w_2}{2} - 1 < w_0 < 1 \end{aligned} \tag{3}$$

The constraints are included by introducing explicit Lagrangian multiplier estimates for each constraint into the objective function. This approach transforms the constrained problem into an unconstrained one, while preserving the feasibility of the solution, as detailed by Jansen and Perez [28].

The gradient-based optimization method used here is the sequential quadratic problem (SQP) method. The SQP method assumes the design space near the optimum to be convex and approximates the nonlinear problem as a quadratic subproblem at each iteration. The optimum corresponding to each quadratic subproblem is then used as the starting point for the next iteration. From the many different SQP implementations available, we select the SNOPT package [30]. The SQP method solves the following subproblem:

$$\begin{aligned} \texttt{minimize} \quad & \tfrac{1}{2} s^T W_k s + g_k^T s \\ \texttt{subject to} \quad & A^T s + \hat{c}_k = 0 \end{aligned} \tag{4}$$

where s is the step size from the current iteration point that minimizes the quadratic subproblem, g_k is the gradient vector of the objective function with respect to the design variables, W_k is the estimate of the second-order derivatives using the Broyden-Fletcher-Goldfarb-Shanno (BFGS) method [31], which is a quasi-Newton method to solve unconstrained nonlinear optimization problems. The matrix A^T is Jacobian of the constraints with respect to the design variables. At each iteration, the solution to the quadratic subproblem is obtained using a quasi-Newton approach.

One of the keys to take full advantage of gradient-based optimization is efficient and accurate computation of derivatives. Given that the battery pack design problem has a relatively small number of variables, the complex-step approximation method [32] is used to obtain the derivatives. The complex-step method is similar to the finite-difference approach of derivative estimation but it has the added advantage of retaining machine precision for arbitrarily small step sizes. The implementation of complex step to obtain derivatives in battery problem is explained in our earlier effort [25].

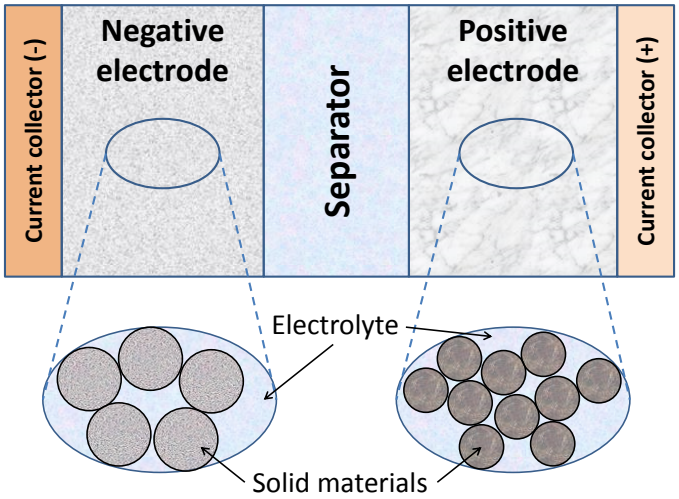

Figure 2: Schematic diagram of a lithium-ion insertion cell

2.2. *Cell model*

Battery analysis starts with a physics-based cell model, and for the work described in this paper, we use a pseudo 2-dimensional cell model that incorporates homogenous electrode formulation with concentrated solution theory [5, 33, 34]. A full sandwich lithium-ion cell (Fig. 2) consisting of porous materials for both the positive and negative electrodes are considered. The porous electrodes, which are comprised of solid active materials and liquid electrolyte, are modeled as a continuum medium [5]. Microstructural effects in the electrodes are ignored and the influence of porosity is instead accounted for using Bruggeman's relation for spherical particles [35]. The model takes into account the key transport processes in both solid and liquid phases and the interfacial reaction rate is modeled using the Butler-Volmer equation. The governing equations for the cell model are listed in Table 1. The state variables solved in the model are the ion concentration in electrolyte, c, and in the solid matrix, c_s, the interfacial current density at the solid matrix surface, i_n, and the potentials in electrolyte and solid matrix, Φ_2 and Φ_1. These state variables in turn provide cell properties that are required in the battery pack model.

State variable	Governing equation
c	$\epsilon\frac{\partial c}{\partial t} = \nabla\cdot\epsilon D\left(1-\frac{d\ln c_o}{d\ln c}\right)\nabla c + \frac{t^o\nabla\cdot\mathbf{i_2}+\mathbf{i_2}\cdot\nabla t^o}{z_+\nu_+F} - \nabla\cdot v_\mathbf{o} + aj_-$
c_s	$\frac{\partial c_s}{\partial t} = \nabla\cdot D_s\left(1-\frac{d\ln c_o}{d\ln c_s}\nabla c_s\right) + \frac{\mathbf{i_1}\cdot\nabla t^o}{z_+\nu_+F} - \nabla\cdot c_s v_o$
$\boldsymbol{i}_n$	$\boldsymbol{i}_n = \boldsymbol{i}_o\left[\exp\left(\frac{\alpha_a F(\phi_1-\phi_2-U)}{RT}\right) - \exp\left(-\frac{\alpha_c F(\phi_1-\phi_2-U)}{RT}\right)\right]$
ϕ_2	$\nabla\phi_2 = -\frac{\boldsymbol{i_2}}{\kappa} + \frac{2RT}{F}(1-t_+^o)\left(1-\frac{d\ln f_\pm}{d\ln c}\right)\nabla\ln c$
ϕ_1	$\boldsymbol{I}-\boldsymbol{i}_2 = -\sigma\nabla\phi_1$

Table 1: Governing equations for a cell model using homogenous electrode formulation and concentrated solution theory.

2.3. Battery model

A simplified battery pack model that consists of identical electrochemical cells arranged in series and parallel is assumed, as shown in Figure 3. There are n modules arranged in series, and each module consists of m layers arranged in parallel. The cells are arranged in such a way that they have to satisfy the safety (voltage and current) constraints. In reality, the cell properties differ slightly due to manufacturing imprecisions, causing variations in cell capacities. As such, accurate battery pack modeling requires each cell to be treated individually [36]. Charge equalization techniques are employed to balance the cells to enhance battery life and to maintain total capacity as well [37, 38]. Variations in cell properties also cause additional difficulties in estimating the battery state of charge (SOC). Various methodologies [39, 40, 41, 42, 43, 44] have been developed to keep track of the SOC in the cells and estimate the remaining capacity.

These additional details in the battery modeling are ignored, as they are not fundamental to the design philosophy outlined in this work. Accounting for these issues would increase the computational burden without shedding new insight into the pack design. However, it should be noted that using the physics-based cell model as the foundation for the pack model would easily allow cell-to-cell variations and accurately reflect intrinsic cell imbalance due to variations in the amount of active materials in the cells [36].

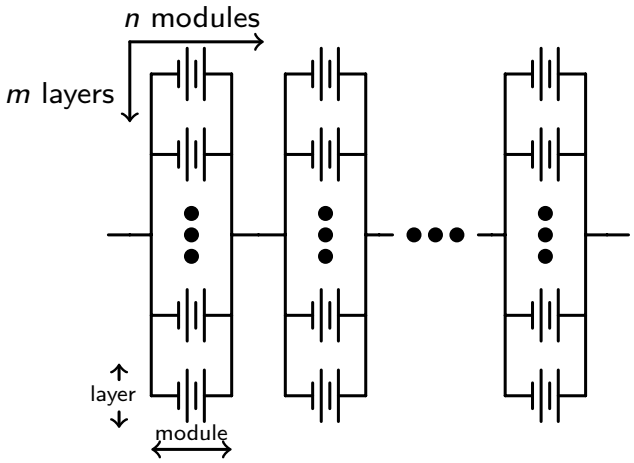

Figure 3: Schematic layout of a battery comprised of uniform cells

3. Problem formulation

PHEV operations require large battery packs of high energy density cells to provide adequate all-electric driving range. Currently only lithium-ion batteries are able to fulfill the requirements. There are various viable lithium-ion electrochemical cells of different energy densities, costs and cycling stability available. A comparison of energy density of various lithium-ion cells using dimensional analysis has been provided by Du et al [45]. For the current work we choose a cell consisting of a lithium-ion cell with spinel manganese oxide $LiMn_2O_4$ for the cathode and mesocarbon microbeads (MCMB) graphite for the anode. Manganese oxide is used as the

cathode material, since it is relatively inexpensive, easily disposable, and exhibits good cycling resistance. The validation of lithium-ion cell with spinel manganese cathode and graphite anode using the cell model outlined in Section 2.2 has been provided by Doyle et al [46]. The fixed properties of the cell are listed in Table 2.

Parameters	**Value**
cathode material	Spinel Mn_2O_4
cathode initial stoichiometric parameter (y in $Li_yMn_2O_4$)	0.2
coulombic capacity of cathode material	148 mAh/g
density of cathode material	4280 kg/m^3
volume fraction of inert filler in cathode	0.1
bulk diffusivity	$10^{-13} m^2/s$
solid particle radius	2 μm
anode material	MCMB 2528 graphite
anode initial stoichiometric parameter (x in Li_xC_6)	0.9
coulombic capacity of anode	372 mAh/g
density of anode material	2260 kg/m^3
volume fraction of inert material in anode	0.05
bulk diffusivity	$10^{-13} m^2/s$
solid particle radius	5 μm
electrolyte material	$LiPF_6$ in EC:DMC
initial salt concentration	1000 mol/m^3
inert filler material	PVDF
ambient temperature	298 K
cycling rate	1.0 C
P-to-N ratio	1.0

Table 2: List of Li-ion cell material properties and fixed parameters [47]

In addition to the fixed variables, six free variables (Table 3) are selected to determine the optimal cell design and pack configuration that best fulfills the pack requirements. These six variables are chosen as they represent design parameters that can be readily manipulated by the battery manufacturer to determine the battery pack properties. There are other parameters such as diffusivity and conductivity as well as electrode particle sizes that affect the performance of the cell. Our earlier work [25] has shown that in the absence of degradation mechanisms and side reactions, these other variables invariably go to the bounds at optimal cell designs. Their relative effects on energy density of the cell have been shown to be less than the morphological parameters chosen for this study [22]. Therefore, they are neglected in this study. Among the six variables, the electrode thicknesses and porosities are morphological parameters that balance the amount of energy content in the cell with the ion transport requirement. A thicker electrode contains more active material for the intercalation process, and hence higher energy capacity. A more porous electrode allows higher rate of ion transport by increasing the effective transport coefficient. However, it reduces the fraction of charge-storing active materials and overall capacity of the cell. The competing effects of higher energy and higher power results in an optimal cell design that must reach a compromise between energy and power. The cutoff voltage determines the lowest SOC in the cell that can still fulfill the power requirement. The peak power available

is dependent on the capacity remaining in the battery and must be accurately determined to avoid over-discharging the battery. While the SOC and cell voltage required to calculate peak power can be conveniently extracted from the cell model in our framework, a more practical approach will involve a multi-parameter, model-based method [48] to estimate the peak power. The last variable is the number of cells connected in parallel within each module, which also determines the maximum current of the pack. The number of modules connected in series is fixed by the maximum voltage of the battery pack, which will be explained in greater detail at the end of this section.

Parameters	Lower bound	Upper bound
cathode thickness (μm)	40.0	250.0
anode thickness (μm)	40.0	250.0
cathode porosity (μm)	0.1	0.6
anode porosity (μm)	0.1	0.6
cut-off voltage (V)	2.6	3.6
no. of layers	1	30

Table 3: List of design variables and their ranges

Three key properties of the battery pack are identified as the objective functions to be minimized, which are the mass, volume and material costs. Each objective can be given as linear functions of the design variables:

$$\begin{aligned} \text{Mass} &= nmA \sum_j \sum_i \epsilon_{ij} \rho_i l_j \\ \text{Volume} &= nmA \sum_j l_j \\ \text{Cost} &= nmA \sum_j \sum_i b_i \epsilon_{ij} \rho_i l_j \end{aligned} \tag{5}$$

where n,m are the number of modules and layers in the battery pack, A is the cross-section of each cell, ϵ, ρ and b are the volume fraction, the mass density and the unit cost [49] of the material respectively, and l is the thickness of the cell component. The index j cycles over the cell components, namely the positive electrode, separator, negative electrode, and the current collectors, while i cycles over the cell materials. Note that if the materials with higher density have higher unit price, then the cost becomes directly correlated with the mass. Reducing the battery pack mass will invariably reduce the cost as well.

Equations (5) show that the objective functions are linear with respect to the design variables. Minimization of the objective functions without proper consideration of constraints simply results in the trivial solution of all design variables at their lower bounds. Therefore, a useful battery pack design requires satisfying appropriate design constraints. These safety and performance requirements impose limits on how close to the lower bounds the design variables can go. The constraints for our problem are listed in Table 4.

The energy of the battery pack is computed by galvanostatic discharge of the cells at 1C cycling rate, while the maximum power is the average power available during a 10-second maximum current pulse at the end of the 1C discharge. The maximum power is computed at the lowest SOC, as this is the point where cell voltage is the lowest. If the battery can meet the power requirement at the end of discharge, it can meet the power requirement throughout its

	Pack				Cell		
Voltage	V_{pack}	$\leq$	400V		$n \cdot V_{cell,init}$	$\leq$	400V
	V_{pack}	$\geq$	280V		$n \cdot V_{cell,end}$	$\geq$	280V
Current	I_{pack}	$\leq$	420A	$\Longrightarrow$	$m \cdot I_{cell}$	$\leq$	420A
Energy	E_{pack}	$\geq$	12kWh		$nm \cdot E_{cell}$	$\geq$	12kWh
Power	P_{pack}	$\geq$	120kW		$nm \cdot P_{cell}$	$\geq$	120kW
Charge balance					Q_+	$=$	Q_-

Table 4: Conversion of pack-level requirements to cell-level constraints

operation. The 10-second current pulse requirement provides a good estimate of the maximum power required for vehicle operation, as it mimics the power demand required for accelerating onto the highway. Based on the constraints outlined in Table 4, the maximum voltage limits the number of battery modules connected in series. The maximum voltage in a cell is the open-circuit voltage at the fully charged state, and the maximum pack voltage divided by this value provides the number of modules allowed in the battery pack. In this study the number of cells connected in series is fixed at 99. The minimum voltage is computed at the end of the 10-second maximum current pulse and it sets the limit on the depth of discharge of the cells. Hence, the optimization problem can be simplified by replacing the voltage constraints with the fixed number of modules in the pack and the minimum cell voltage to terminate discharge.

4. Results and discussion

4.1. Discharge profile

A typical discharge profile obtained from the cell-model simulation is shown in Figure 4, which shows both the cell voltage and the current density profiles. The small insert in Figure 4 shows the voltage and current profile at the transition between the galvanostatic discharge and peak power current pulse. The sudden jump in the cell current creates a discontinuity in the voltage profile. The cell voltage decreases rapidly as the amount of charge is depleted at a greater rate.

The secant method is used to obtain the maximum current during the 10-second pulse. The maximum current is defined as the largest current required for maintaining the minimum voltage at the end of the pulse. The iterative process for the maximum current computation is shown in Figure 5. The final cell voltage decreases monotonically as the pulse current is increased, and the negative correlation between the maximum current and the final cell voltage is shown in the insert.

4.2. Optimization results

As mentioned previously, three different optimization problems are solved using the optimization framework to design the PHEV battery pack: 1) to minimize battery mass, 2) to minimize battery volume, and 3) to minimize battery material cost. The six design variables are listed in Table 3 and the four constraints are presented in Table 4. To compare the performance of the optimized cell designs, three simple initial pack designs are selected. The first two designs follow the general 'ad-hoc' guidelines for cell electrode design; the first one is a power cell with thin electrode and high porosity, and the other is an energy cell with thick electrode and low

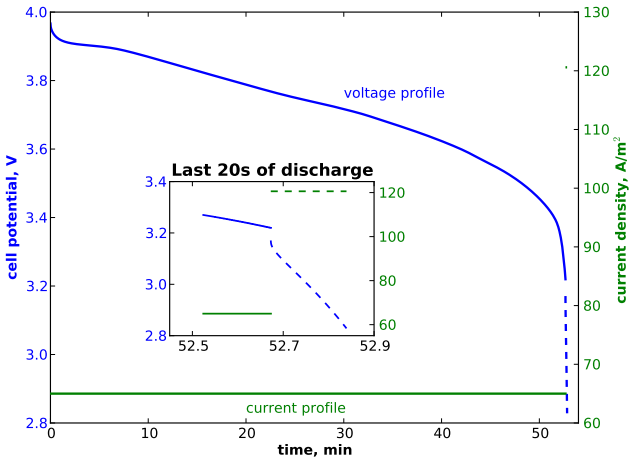

Figure 4: Discharge profile for a lithium-ion cell undergoing 1C constant current discharge (main) followed by a 10-second peak power pulse at the end of the discharge (insert)

porosity. The third one is based on the earlier work of cell optimization subjected to a power constraint [25]. The optimized cell selected for comparison is designed at the same power-to-energy ratio as specified in the problem definition for the PHEV battery pack. The difference between the single cell and pack design philosophy is that single cell optimization is performed at one discharge rate, while the power and energy requirement for the pack design are performed at different discharge rates, resulting in additional constraints in the design problem. The specifications for the three initial designs and their properties are listed in Table 5. All three initial designs satisfy the capacity balance requirement imposed on the problem.

Analyses of initial pack designs show that the optimized single cell and power cell designs have similar properties, with the power cell exhibiting slightly better performance. The energy cell design is the worst among the three, as its thick electrodes and low porosity result in an expensive and bulky cell without providing any energy density improvement over the other two. All three initial pack designs require 13 layers of cells in parallel to satisfy the pack constraints. This results in the energy cell designs being the heaviest, most voluminous, and most expensive.

Given that the three separate objective functions are not linear combinations of one another, the optimal design for one objective should not be the optimum for another. Table 5 shows that the power cell design performs the best for all three objectives, it is thus not expected to be the true optimal design. In addition, while the power requirement of the pack is exceeded, the energy capacity requirement is not fully satisfied by any of the three initial designs. Therefore, further improvement is possible and can be achieved using numerical optimization.

The gradient-free optimization is first carried out to obtain an approximate estimate of the optimal design and to determine the integer value of cell layers. A representative iteration history of cost optimization is shown in Figure 6. Note that the ALPSO is a population-based optimization method such that at each iteration, there are multiple design points existing simultaneously. The plots shown here contain only the design point that best satisfies the design problem criteria at each iteration, evaluated by the Lagrange function for each particle [28].

Subplots a, b and c in Figure 6 show how the six design variables change during the iteration

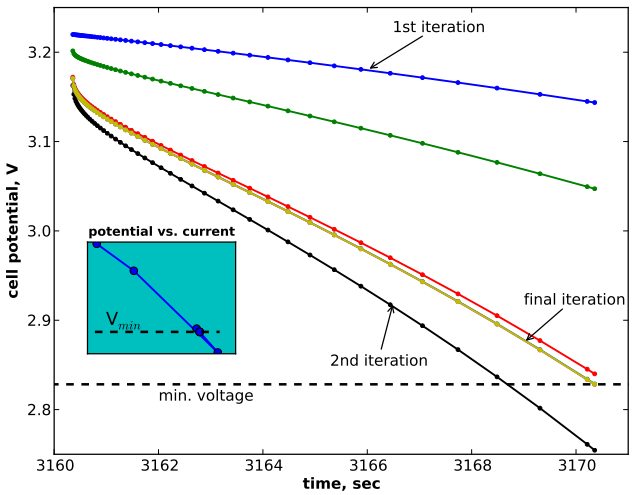

Figure 5: Discharge profiles of the 10-second peak current phase. The secant method is used to determine the maximum current such that the cell potential is exactly at the minimum voltage at the end of the discharge (insert)

while subplot 6d shows the evolution of the objective function (solid line) and the normalized constraint values (dashed lines) during the optimization process. The normalized constraint value is given as a percentage, with 100% and above indicating that the constraint is satisfied. The charge balance constraint is an equality constraint that has to be satisfied exactly at all times and hence is not plotted. The optimization history shown in Figure 6 can be broken down into three phases. The initial design has high number of layers and this resulted in a high battery cost and extremely high current. The first six iterations reduced the number of layers and hence lowered the current to below the maximum allowed value, however this results in energy and power requirements being not satisfied. Further adjustment of the design variables in the next five iterations converged close to the final cell design, which shows that the energy and power constraints are fulfilled exactly, while the maximum current is well above the maximum allowed level. Given the competing effects of energy and power in the battery cell, this result is expected, as the optimal cell design would be one that satisfies but does not exceed both requirements.

ALPSO is a stochastic optimization method, hence multiple optimizations runs were performed for each optimization problem. The best results are listed in Table 6. Optimizing for mass and material costs results in very similar optimal cell designs. In fact, the optimal design obtained for cost minimization has the lowest battery pack mass as well. Given that reduction in battery mass naturally leads to less materials and hence lower cost, this result is not surprising. While the difference between the minimal-mass weight and minimal-cost weight is within the convergence tolerance of the optimizer, it also indicates the ALPSO is unable to locate the true optima in this situation, such that the final result found for mass minimization problem is sub-optimal.

A comparison between Tables 5 and 6 shows decreases of 13.4%, 18.1%, and 17.9% in mass, volume and cost respectively from initial to optimal designs. Compared with the best initial cell designs, all three optimal designs have thicker electrodes and lower porosities. Therefore each cell has higher energy density, while still satisfying the power requirement. The energy and

	power cell	energy cell	optimized single cell
cathode thickness (μm)	129.9	189.8	141.7
anode thickness (μm)	80.0	120.0	70.0
cathode porosity	0.4	0.2	0.442
anode porosity	0.4	0.2	0.322
cutoff voltage (V)	3.53	3.63	3.53
no of layers	13	13	13
mass (kg)	86.89	126.00	87.14
volume (dm^3)	29.34	39.62	29.52
cost ($)	1398	1862	1401
energy capacity [$\geq$ 12kWh]	11.9	11.8	11.9
maximum current [$\leq$ 420A]	388.0	385.2	389.3
peak power [$\geq$ 120kW]	121.5	123.3	121.7

Table 5: Battery cell properties of initial designs

power requirements are satisfied with far fewer cells (9 or 10 layers vs. 13), and hence better overall pack properties.

There are some differences between the three optimized designs. The mass and cost minimization problems produce optimal cell designs that have thick electrodes, such that the cell has as much active material for lithium ion intercalation as possible. This is to maximize the energy density of the cell and to reduce the total amount of materials needed. While cost minimization problem results in a battery pack lighter than the one obtained from the mass minimization problem, the difference is within the convergence tolerance of ALPSO. Volume minimization, on the other hand, produces an optimal cell design that has thinner electrodes with lower porosities. This results in a cell design that has lower gravimetric energy density, but higher volumetric energy density compared to the designs for the other two problems.

The optimal cell designs are further improved by using SNOPT to refine the continuous cell variables. The gradient-based optimization is initiated at the optimal designs obtained from ALPSO. The number of layers in each module, which is a discrete variable, is fixed at the values around the optimal number of layers obtained via ALPSO, while the gradient-based optimizer fine-tunes the continuous variables. The results obtained using SNOPT are listed in Table 7. Again we notice the similarity between the mass minimization and cost minimization solutions. The two optimal designs are almost identical, and the material cost difference between the two is less than one dollar. The volume minimization problem produces a battery pack with much thinner electrodes and lower porosities. Comparing the SNOPT and ALPSO volume minimization results, the cathode and anode thicknesses are 21.3% and 25.6% thinner respectively while the porosities are 19.1% and 40.5% less. The number of cells required increases by 20%. The low electrode porosity means the cell design is less adequate to handle high discharge rate, however this is alleviated by having a larger number of cells connected in parallel and hence a smaller current density through each cell. The SNOPT optimal design has higher mass and material cost but lower volume. While utilizing larger number of cells with lower energy density may seem counter-intuitive, it demonstrates the ability of the optimizer to drive the design to achieve the objective, which in this particular instance is to minimize the volume of the pack.

Results in Table 7 show that improvements from gradient-free optmization to gradient-based

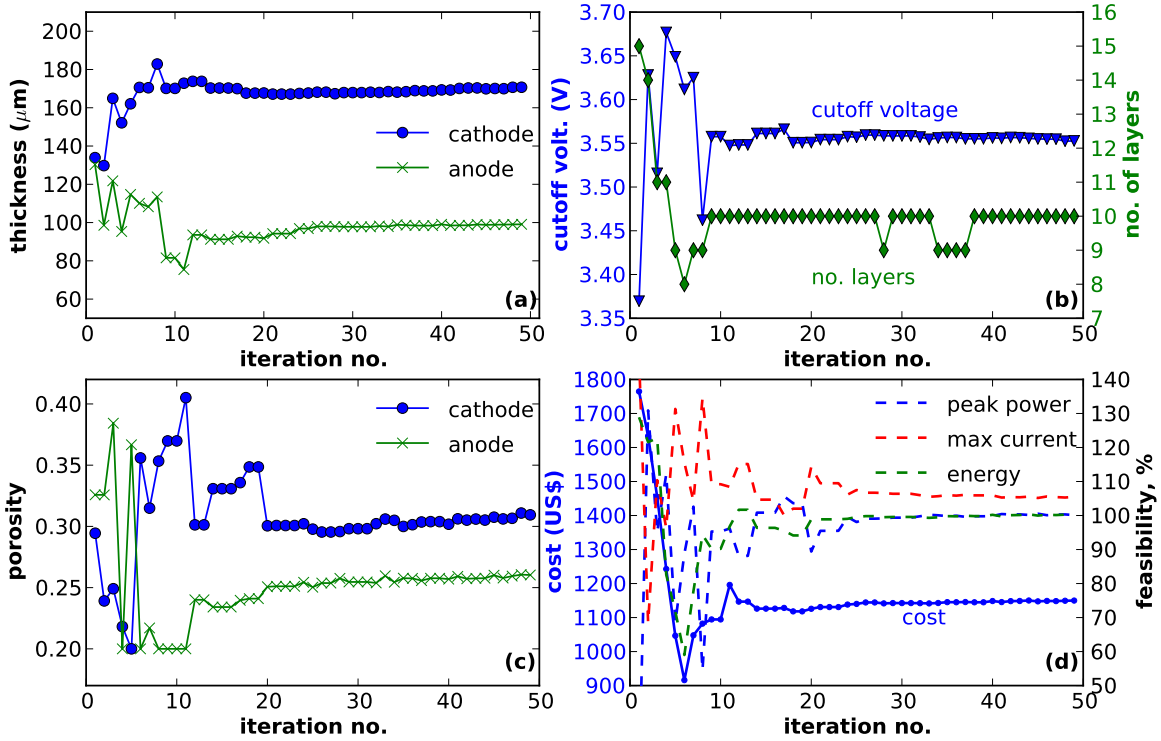

Figure 6: Iteration history of an optimization to minimize battery cost showing the evolution of: a) electrode thicknesses, b) cutoff-voltage and no of layers, c) electrode porosities, and d) cost and normalized inequality constraint values

optimization results are less than 1% for all three optimization problems. This is mainly due to the flatness of the design space near the optimum, and there is little gain in pinpointing the exact location of the optimal designs, as evidenced by the 8% difference in negative electrode porosity between ALPSO and SNOPT results. Such differences, however, may become more important as more details about cell modeling are included. For instance, manganese dissolution rate has been shown to correlate to the interfacial surface area in the porous electrode [50]. Increase in cathode porosity will increase interfacial surface area and could potentially cause accelerated cell degradation. Inclusion of additional degradation mechanisms will likely add nonlinearity to the design space and further restricts the feasible design regions.

One common problem with gradient-based optimization is that it often converges to local optimum solutions instead of global best ones. To show that the solutions are indeed global optimal and that the design space near the solutions are not dominated by local optima, we obtain the contour plots of the objective functions on the plane that passes through the three optimal design points of mass, volume and cost respectively. The plane is obtained by projecting the design space onto the plane spanned by the coordinates of the three optimal design points. The three optimal points are transformed into the non-dimensional coordinates $(0,0),(1,0),(0,1)$ respectively on the plane. The shaded area on Figure 7 indicates the region where the energy, power, voltage and current requirements are all concurrently satisfied. The blue curve indicates

Properties	Objective function		
	Mass	Volume	Cost
mass (kg)	74.97	75.67	<u>74.90</u>
volume (dm^3)	24.91	<u>24.02</u>	24.48
cost ($)	1153	1169	<u>1147</u>
cathode thickness (μm)	169.8	141.9	168.8
anode thickness (μm)	104.7	86.4	99.8
cathode porosity	0.321	0.272	0.305
anode porosity	0.314	0.252	0.269
cutoff voltage (V)	3.52	3.53	3.53
no of layers	9	10	9
energy capacity [$\geq$ 12kWh]	12.0	12.0	12.0
maximum current [$\leq$ 420A]	398.4	395.0	396.6
peak power [$\geq$ 120kW]	120.1	119.9	120.1

Table 6: Preliminary designs after gradient-free optimization. Results shown are the 'best-available' ones due to stochastic nature of ALPSO algorithms.

the narrow band that fulfills the charge balance requirement, while the black lines show the design space that satisfies the integer requirement imposed on the number of layers.

In the plots shown in Figure 7, we can see that the objective functions vary smoothly in the feasible design space. The mass and cost contours vary monotonically in the feasible design space, while there is a local volume maximum for the volume contour plot. All three optimal design points are located on the boundary of the feasible space, again confirming that the constraints are active in this design problem. The location of the optimal designs are further restricted by the charge capacity equality constraints and the integer requirement on the number of cell layers. Based on the information available in Figure 7, it is clear that the optimal designs are indeed the best possible designs in the slice of plane shown here. Such information, together with the smoothness of the objective functions, gives us confidence about the global optimality of the results. The similarity between mass and cost optimal designs can also be explained from the contour plots in Figure 7. Comparison of the mass and cost contours reveal that the two objectives are very similar to one another in the given plane. The gradients for both objectives point in the same x-direction, and in both cases the best objective functions are on the left boundary of the feasible space. The similarities of the objectives result in mass and cost optimal designs being very close to each other in the actual design space.

The optimal cell design for mass minimization problem is compared with the optimal single-cell design from our previous work [25], in which the optimal cell has the maximum energy density at constrained discharge rates. Comparison to the optimal cell at 1C discharge rate shows the PHEV pack cell design has thinner electrodes and higher porosities. This is due to the additional peak power requirement at the end of discharge, which imposes a higher ion transport requirement. The resulting cell design, while not optimal in term of energy density, is able to meet both the energy and power requirements simultaneously, which is more important given the variations in power demand under normal driving conditions.

Properties	Objective function		
	Mass	Volume	Cost
mass (kg)	74.77	79.53	75.06
volume (dm^3)	24.49	23.85	24.37
cost ($)	1146	1241	1146
cathode thickness (μm)	169.2	111.7	169.4
anode thickness (μm)	99.4	64.3	97.5
cathode porosity	0.310	0.220	0.300
anode porosity	0.270	0.150	0.245
cutoff voltage (V)	3.53	3.55	3.54
no of layers	9	12	9
energy capacity [$\geq$ 12kWh]	12.0	12.0	12.0
maximum current [$\leq$ 420A]	395.9	392.5	394.4
peak power [$\geq$ 120kW]	119.9	120.1	119.8

Table 7: Refined optimal designs obtained using gradient-based optimizations

Properties	Values
vehicle mass (kg)	1500
passenger mass (kg)	150
rolling resistance coeff.	0.01
drag coefficient	0.30
frontal area (m^2)	2.0
motor efficiency	0.85
drivetrain efficiency	0.8
generator efficiency	0.85
regenerative braking factor	0.1

Table 8: Properties of the vehicle used to complete the driving cycle

4.3. Driving cycle test

While the optimal designs obtained using the aforementioned optimization framework show better overall properties than the initial design, it is important to show that they translate to actual performance advantage in the PHEV operations. We next compare the performance of the battery packs by simulating discharge using standard federal testing driving cycles. A standard sedan with the properties listed in Table 8 is used to compute the battery power required to complete the driving cycles. The power needed to follow the driving cycle at any particular time instance is given as:

$$P_{tot} = P_{acc} + P_{drag} + P_{roll} + P_{mis} \tag{6}$$

where the total power required is the sum of the power required to overcome aerodynamic forces (P_{drag}), rolling resistance(P_{roll}), power miscellaneous systems (P_{mis}) and to achieve the required acceleration (P_{acc}) of the driving cycle. The miscellaneous power refers to the power required for various auxiliary systems not related to drivetrain and it is given the constant value of 1.0 kW. Using Equation 6, the power required for any driving cycle can be computed.

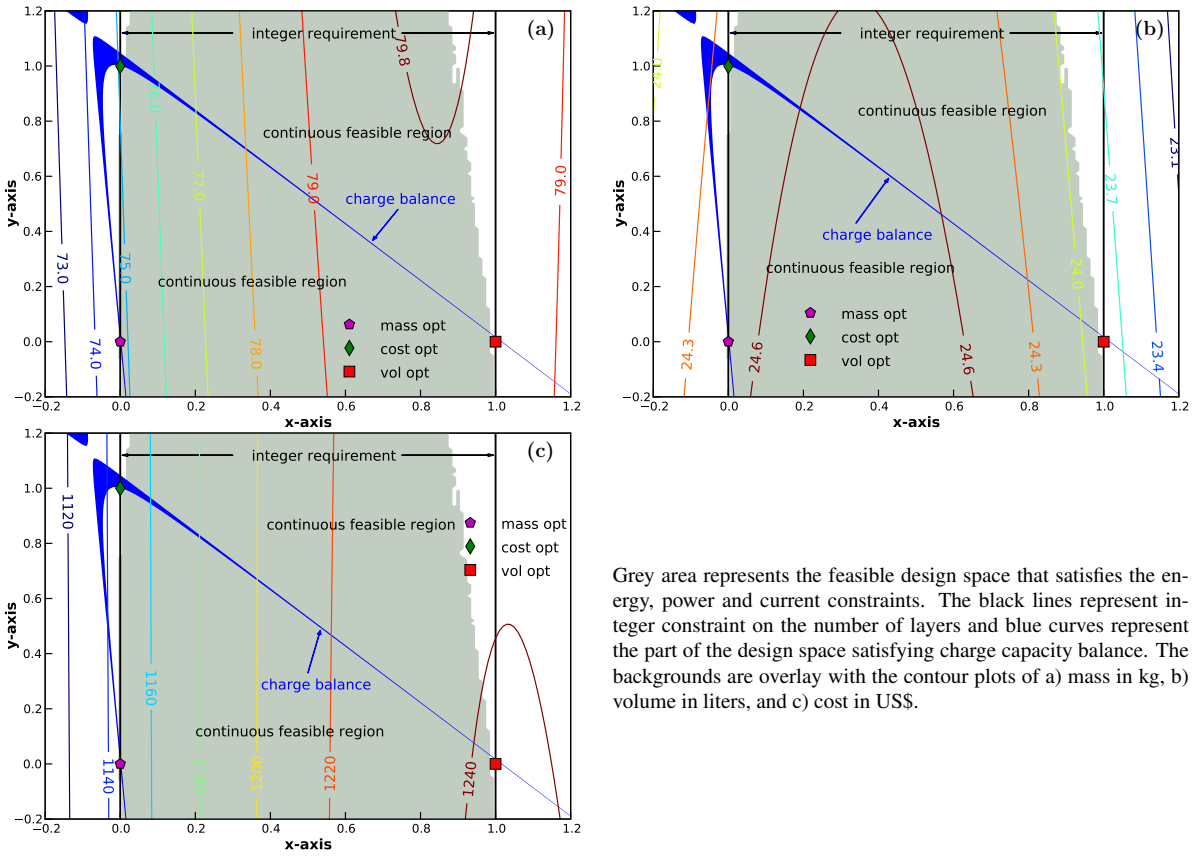

Grey area represents the feasible design space that satisfies the energy, power and current constraints. The black lines represent integer constraint on the number of layers and blue curves represent the part of the design space satisfying charge capacity balance. The backgrounds are overlay with the contour plots of a) mass in kg, b) volume in liters, and c) cost in US$.

Figure 7: Contour plots of objective functions on the plane spanning the three optimal design points

The battery packs are discharged through the three standard federal driving cycles: UDDS, SC03 and US06, with their speed and corresponding power profiles shown in Figure 8. The UDDS and SC03 cycles both mimic city driving conditions, with SC03 being slightly more aggressive. US06 simulates highway driving condition. The highway acceleration requirements impose higher power demands on the battery, with power demands peaking at 100 kW. The battery is discharged from an initial SOC of approximately 0.8 until the minimum voltage of 280V is reached and the total distance covered for each of the driving cycle is calculated.

Both the initial design and optimal battery packs are discharged through the simulated driving cycles. The voltage and SOC profiles of the mimimum mass optimal battery pack and the initial design discharged through the simulated US06 driving cycle are shown in Figure 9. The open-curcuit voltage (OCV) curve is plotted on the same figure for comparison. The SOC profile shows that the optimal battery pack lasts longer than the initial design battery pack, resulting in 3.5% longer electric range. The initial battery design contains more cells in parallel compared to the optimal battery pack, therefore each cell is subjected to a smaller current density. This results in higher battery pack voltage in the initial design, and less energy lost per cell due to internal resistance. However, the higher energy density of the optimal battery pack cells still result in overall better performance.

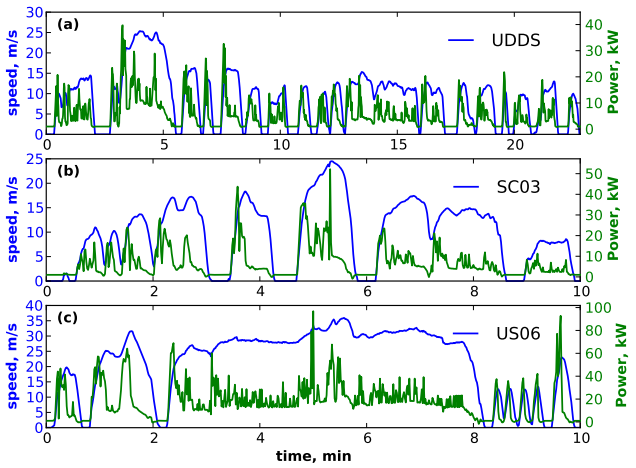

Figure 8: Federal driving cycle speed profiles and the corresponding battery power requirement

	Battery design			
Drive cycle	Initial	Min. mass	Min. volume	Min. cost
UDDS	53.7 km	57.2 km	58.1 km	58.1 km
SC03	48.6 km	52.5 km	53.4 km	53.4 km
US06	39.7 km	41.1 km	42.1 km	41.8 km

Table 9: All electric driving range for various battery designs

The all electric ranges for various battery pack designs subject to the three driving cycles are listed in Table 9. For all three driving cycles, the optimal battery pack designs outperform the initial battery pack designs in terms of all-electric range. The most improvement is in SC03 cycle discharge, with the electric ranges of minimum-volume and minimum-cost battery packs almost 10% better than that of the initial design.

While the electric driving range of the optimal battery pack designs show significant improvement over the initial design, a better measure of the battery performance would be to measure the distance travelled per unit of battery performance metric, where the metric is either mass, volume or material cost. Figure 10 compares the performance of the optimal battery designs with the best initial design. While the initial and optimal designs have similar all-electrice drive range, the optimal designs clearly have better performance per unit of battery performance metric. On average, the optimal battery packs show 23.1% improvement in distance per unit of battery mass, 32.8% improvement in distance per unit volume and 31.4% improvement in distance per unit cost.

Results in Table 9 also shows that the minimum-volume battery pack has the longest electric ranges among the optimal battery pack designs. The disparity between the electric driving ranges of the various optimal battery packs demonstrates that while the battery packs satisfy similiar energy and power requirements, the performance is dependent on the driving cycle, or control variables governing the discharge of the battery. This points to the possible advantages of

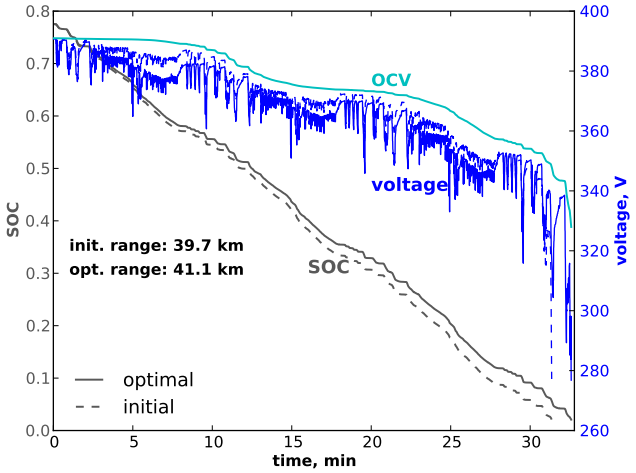

Figure 9: Comparison of the voltage and SOC profiles of the initial design and minimum-mass optimal battery pack discharged through the simulated US06 driving cycle

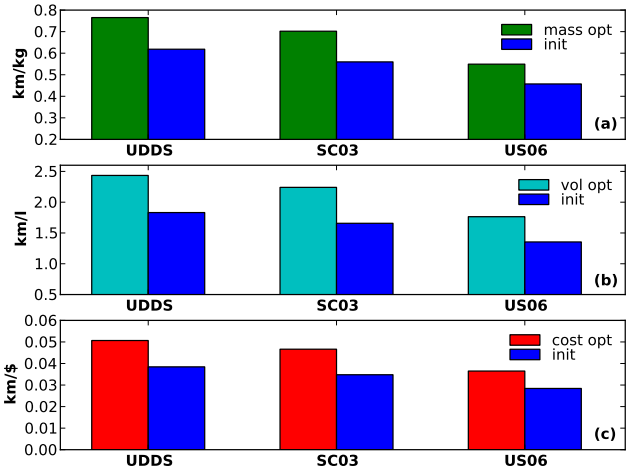

Figure 10: Comparison of battery performance between initial and optimal designs using driving cycle data

performing a design-control coupled optimization. In addition, we only consider the all-electric operating mode of the PHEV drive and not the overall performance of the PHEV. The problem definition is limited to minimizing the properties of the battery pack, and this allows decoupling of the battery from other drivetrain components. To truly optimize the operation of the PHEV, the hybrid mode, during which both engine and electric power are in use, needs to be considered as well. The degree of hybridization in the PHEV, which is the ratio of electric motor power to the total drivetrain power, is shown to affect the optimality of the drivetrain components performance [51]. Therefore, the overall hybridization scheme of a PHEV is defined by the battery, electric motor and internal combustion engine collectively [14]. Inclusion of various components also necessitates the coupling of power control strategies with design parameters to determine the optimal performance. Kim and Peng [18] has shown that the "power management and design" optimization showed a 17% improvement in fuel economy over "power management only" results. Consideration of the engine and electric motor sizes could allow for battery design that best meets the peak power demand during climbing and acceleration, and keeps the engine operation at maximum efficiency.

5. Conclusions

This work outlines a methodology to perform battery design optimization by coupling a numerical optimization framework with a physics-based electrochemical cell model. Given the nonlinear and mixed-integer nature of the optimization problem, a hybrid optimization approach was developed. A gradient-free optimizer is first used to obtain an approximate estimate of the optimal design and to obtain the optimal integer design variables. The design is then further refined using the gradient-based optimization. Such a framework is very useful to obtain the best possible initial designs, from which further refinement can be carried out by accounting for additional details such as degradation mechanisms and manufacturing constraints. Comparisons between the initial and optimal designs show overall improvements of 13.9%, 18.7% and 18.0% in battery mass, volume and cost, respectively. The optimal designs also perform better in real drive cycle simulations. The improvements in battery pack properties can be translated to 23.1% increase in distance traveled per unit mass, 32.8% increase in distance per unit volume, and 31.4% increase in distance per unit cost. The electrochemical cell in this case is assumed to be ideal and additional capacity fade mechanisms should be considered in the future.

Acknowledgements

The present efforts were supported by the General Motors and University of Michigan Advanced Battery Coalition for Drivetrains (ABCD). All computations were performed on the FLUX high-performance computing network, sponsored by the College of Engineering, University of Michigan.

List of Symbols

Electrochemistry variables

a	interfacial surface area
A	cross-section area of an electrochemical cell

b	material unit cost
c	salt concentration in electrolyte
c_s	salt concentration in solid matrix
D	diffusion coefficient of electrolyte
D_s	diffusion coefficient of solid matrix
$f_\pm$	mean molar activity coefficient of electrolyte
F	Faraday's constant
i_n	transfer current density at the surface of active material
i_o	exchange current density
i_2	current density in electrolyte
l	thickness
m	number of electrochemical cell in parallel
n	number of electrochemical cell in series
Q	charge capacity
R	universal gas constant
T	temperature
U	surface overpotential
α_a, α_c	anodic and cathodic transfer quotient
ϵ	volume fraction
κ	ionic conductivity in electrolyte
σ	ionic conductivity in solid matrix
Φ_1	potential in solid matrix
Φ_2	potential in electrolyte
ρ	material density

Subscripts

o	initial state value
s	value in solid matrix
$+$	positive electrode
$-$	negative electrode

Optimization variables

A	Jacobian of constraints w.r.t. design variables
c_j	inequality constraints
$\hat{c}_k$	equality constraints
g	gradient vector of objective w.r.t. design variables
p^i	best position of the ith particle
p^g	global best position
r_1, r_2	random numbers between 0 and 1
s	solution to the quadratic subproblem in SQP
V	velocity of particle in design space
w_0	inertia weight in ALPSO
w_1, w_2	confidence parameters in ALPSO
W	estimate of second-order derivatives in SQP
$\boldsymbol{x}$	position of particle in design space
Δt	time step value in ALPSO, normally taken to be 1

References

[1] M. Ehsani, Y. Gao, J. M. Miller, Hybrid electric vehicles: architecture and motor drives, Proceedings of the IEEE 95 (4) (2007) 719–728.

[2] B. Scrosati, J. Garche, Lithium batteries: status, prospects and future, J Power Sources 195 (9) (2010) 2419–2430.

[3] C. Sandy Thomas, Transportation options in a carbon-constrained world: Hybrids, plug-in hybrids, biofuels, fuel cell electric vehicles, and battery electric vehicles, Int J Hydrogen Energ 34 (23) (2009) 9279–9296.

[4] M. Alamgir, A. M. Sastry, Efficient batteries for transportation applications, SAE Paper (2008) 21–0017.

[5] M. Doyle, T. F. Fuller, J. Newman, Modeling of galvanostatic charge and discharge of the lithium/polymer/insertion cell, J Electrochem Soc 140 (6) (1993) 1526–1533.

[6] M. Valvo, F. E. Wicks, D. Robertson, S. Rudin, Development and application of an improved equivalent circuit model of a lead acid battery, in: Energy Conversion Engineering Conference, 1996. IECEC 96., Proceedings of the 31st Intersociety, Vol. 2, IEEE, 1996, pp. 1159–1163.

[7] B. Yann Liaw, G. Nagasubramanian, R. G. Jungst, D. H. Doughty, Modeling of lithium ion cells - a simple equivalent-circuit model approach, Solid State Ionics 175 (1) (2004) 835–839.

[8] W. Gu, C. Wang, B. Liaw, The use of computer simulation in the evaluation of electric vehicle batteries, J Power Sources 75 (1) (1998) 151–161.

[9] M. W. Verbrugge, R. S. Conell, Electrochemical and thermal characterization of battery modules commensurate with electric vehicle integration, J Electrochem Soc 149 (1) (2002) A45–A53.

[10] V. Ramadesigan, P. W. Northrop, S. De, S. Santhanagopalan, R. D. Braatz, V. R. Subramanian, Modeling and simulation of lithium-ion batteries from a systems engineering perspective, J Electrochem Soc 159 (3) (2012) R31–R45.

[11] A. Cooper, Development of a lead-acid battery for a hybrid electric vehicle, J Power Sources 133 (1) (2004) 116–125.

[12] B. Y. Liaw, M. Dubarry, From driving cycle analysis to understanding battery performance in real-life electric hybrid vehicle operation, J Power Sources 174 (1) (2007) 76–88.

[13] M. Dubarry, V. Svoboda, R. Hwu, B. Y. Liaw, A roadmap to understand battery performance in electric and hybrid vehicle operation, J Power Sources 174 (2) (2007) 366–372.

[14] S. K. Shahi, G. G. Wang, L. An, E. Bibeau, Z. Pirmoradi, Using the pareto set pursuing multiobjective optimization approach for hybridization of a plug-in hybrid electric vehicle, J Mech Design 134 (2012) 094503–1–6.

[15] X. Wu, B. Cao, X. Li, J. Xu, X. Ren, Component sizing optimization of plug-in hybrid electric vehicles, Appl Energ 88 (3) (2011) 799–804.

[16] Y.-H. Hung, C.-H. Wu, An integrated optimization approach for a hybrid energy system in electric vehicles, Appl Energ 98 (2012) 479–490.

[17] Y. Zou, F. Sun, X. Hu, L. Guzzella, H. Peng, Combined optimal sizing and control for a hybrid tracked vehicle, Energies 5 (11) (2012) 4697–4710.

[18] M.-J. Kim, H. Peng, Power management and design optimization of fuel cell/battery hybrid vehicles, J Power Sources 165 (2) (2007) 819–832.

[19] K. Darcovich, E. Henquin, B. Kenney, I. Davidson, N. Saldanha, I. Beausoleil-Morrison, Higher-capacity lithium ion battery chemistries for improved residential energy storage with micro-cogeneration, Appl Energ 111 (0) (2013) 853 – 861. doi:http://dx.doi.org/10.1016/j.apenergy.2013.03.088.

[20] J. Newman, Optimization of porosity and thickness of a battery electrode by means of a reaction-zone model, J Electrochem Soc 142 (1) (1995) 97–101.

[21] C. Fellner, J. Newman, High-power batteries for use in hybrid vehicles, J Power Sources 85 (2) (2000) 229–236.

[22] W. Du, A. Gupta, X. Zhang, A. M. Sastry, W. Shyy, Effect of cycling rate, particle size and transport properties on lithium-ion cathode performance, Int J Heat Mass Trans 53 (17) (2010) 3552–3561.

[23] V. Ramadesigan, R. N. Methekar, F. Latinwo, R. D. Braatz, V. R. Subramanian, Optimal porosity distribution for minimized ohmic drop across a porous electrode, J Electrochem Soc 157 (12) (2010) A1328–A1334.

[24] S. Golmon, K. Maute, M. L. Dunn, Multiscale design optimization of lithium ion batteries using adjoint sensitivity analysis, Int J Numer Methods Eng 92 (5) (2012) 475–494.

[25] N. Xue, W. Du, A. Gupta, W. Shyy, A. M. Sastry, J. R. R. A. Martins, Optimization of a single lithium-ion battery cell with a gradient-based algorithm, J Electrochem Soc 160 (8) (2013) A1071–A1078.

[26] D. Sumitava, P. W. Northrop, V. Ramadesigan, V. R. Subramanian, Model-based simultaneous optimization of multiple design parameters for lithium-ion batteries for maximization of energy density, J Power Sources 227 (2013) 161–170.

[27] A. B. Lambe, J. R. R. A. Martins, Extensions to the design structure matrix for the description of multidisciplinary design, analysis, and optimization processes, Struct Multidiscip O 46 (2012) 273–284. doi:10.1007/s00158-012-0763-y.

[28] P. W. Jansen, R. E. Perez, Constrained structural design optimization via a parallel augmented Lagrangian particle

swarm optimization approach, Comput Struct 89 (2011) 1352–1366. doi:10.1016/j.compstruc.2011.03.011.
[29] R. E. Perez, P. W. Jansen, J. R. R. A. Martins, pyOpt: a Python-based object-oriented framework for nonlinear constrained optimization, Struct Multidiscip O 45 (1) (2012) 101–118. doi:10.1007/s00158-011-0666-3.
[30] P. Gill, W. Murray, M. Saunders, SNOPT: An SQP algorithm for large-scale constraint optimization, SIAM J Optimiz 12 (4) (2002) 979–1006.
[31] J. Nocedal, S. J. Wright, Numerical Optimization, 2nd Edition, Springer, 2006.
[32] J. R. R. A. Martins, P. Sturdza, J. J. Alonso, The complex-step derivative approximation, ACM T Math Software 29 (3) (2003) 245–262. doi:10.1145/838250.838251.
[33] K. Thomas, J. Newman, R. Darling, Mathematical modeling of lithium batteries, Advances in Lithium-ion Batteries (2002) 345–392.
[34] J. Newman, K. E. Thomas-Alyea, Electrochemical Systems, Wiley-Interscience, 2004.
[35] V. D. Bruggeman, Berechnung verschiedener physikalischer konstanten von heterogenen substanzen. i. dielektrizitätskonstanten und leitfähigkeiten der mischkörper aus isotropen substanzen, Annalen der Physik 416 (7) (1935) 636–664.
[36] M. Dubarry, N. Vuillaume, B. Y. Liaw, From single cell model to battery pack simulation for Li-ion batteries, J Power Sources 186 (2) (2009) 500–507.
[37] Y.-S. Lee, M.-W. Cheng, Intelligent control battery equalization for series connected lithium-ion battery strings, Industrial Electronics, IEEE Transactions on 52 (5) (2005) 1297–1307.
[38] S. W. Moore, P. J. Schneider, A review of cell equalization methods for lithium ion and lithium polymer battery systems, SAE Publication (2001) 01–0959.
[39] C. Hu, B. D. Youn, J. Chung, A multiscale framework with extended Kalman filter for lithium-ion battery SOC and capacity estimation, Appl Energ 92 (0) (2012) 694 – 704. doi:http://dx.doi.org/10.1016/j.apenergy.2011.08.002.
[40] H. Dai, X. Wei, Z. Sun, J. Wang, W. Gu, Online cell SOC estimation of Li-ion battery packs using a dual time-scale Kalman filtering for EV applications, Appl Energ 95 (0) (2012) 227 – 237. doi:http://dx.doi.org/10.1016/j.apenergy.2012.02.044.
[41] L. Zhong, C. Zhang, Y. He, Z. Chen, A method for the estimation of the battery pack state of charge based on in-pack cells uniformity analysis, Appl Energ 113 (0) (2014) 558 – 564. doi:http://dx.doi.org/10.1016/j.apenergy.2013.08.008.
[42] R. Xiong, F. Sun, Z. Chen, H. He, A data-driven multi-scale extended kalman filtering based parameter and state estimation approach of lithium-ion olymer battery in electric vehicles, Appl Energ 113 (0) (2014) 463 – 476. doi:http://dx.doi.org/10.1016/j.apenergy.2013.07.061.
[43] Y. Xing, W. He, M. Pecht, K. L. Tsui, State of charge estimation of lithium-ion batteries using the open-circuit voltage at various ambient temperatures, Appl Energ 113 (0) (2014) 106 – 115. doi:http://dx.doi.org/10.1016/j.apenergy.2013.07.008.
[44] Y. Zheng, M. Ouyang, L. Lu, J. Li, X. Han, L. Xu, H. Ma, T. A. Dollmeyer, V. Freyermuth, Cell state-of-charge inconsistency estimation for LiFePO4 battery pack in hybrid electric vehicles using mean-difference model, Appl Energ 111 (0) (2013) 571 – 580. doi:http://dx.doi.org/10.1016/j.apenergy.2013.05.048.
[45] W. Du, N. Xue, A. M. Sastry, J. R. Martins, W. Shyy, Energy density comparison of Li-ion cathode materials using dimensional analysis, J Electrochem Soc 160 (8) (2013) A1187–A1193.
[46] M. Doyle, J. Newman, A. S. Gozdz, C. N. Schmutz, J.-M. Tarascon, Comparison of modeling predictions with experimental data from plastic lithium ion cells, J Electrochem Soc 143 (6) (1996) 1890–1903.
[47] M. Park, X. Zhang, M. Chung, G. B. Less, A. M. Sastry, A review of conduction phenomena in Li-ion batteries, J Power Sources 195 (24) (2010) 7904–7929.
[48] F. Sun, R. Xiong, H. He, W. Li, J. E. E. Aussems, Model-based dynamic multi-parameter method for peak power estimation of lithiumion batteries, Appl Energ 96 (0) (2012) 378 – 386. doi:http://dx.doi.org/10.1016/j.apenergy.2012.02.061.
[49] K. G. Gallagher, D. Dees, P. Nelson, Phev battery cost assessment (2011).
[50] D. H. Jang, Y. J. Shin, S. M. Oh, Dissolution of spinel oxides and capacity losses in 4 V Li/$Li_xMn_2O_4$ cells, J Electrochem Soc 143 (7) (1996) 2204–2211.
[51] J. Larminie, J. Lowry, Electric vehicle technology explained, Wiley Online Library, 2012.